



## CALCULATION OF WALL HEAT FLUXES FOR THE SUB-ORBITAL SARA CAPSULE ATMOSPHERIC FLIGHT

**Carlos Junqueira-Junior**

Instituto Tecnológico de Aeronáutica, São José dos Campos, Brazil  
junior.hmg@gmail.com

**Fernanda Regina da Conceição Barreto**

Universidade Federal do ABC, Santo André, Brazil  
reginabarreto@hotmail.com

**João Luiz F. Azevedo**

**Humberto Araujo Machado**

**Edson Basso**

**José Guido Damilano**

Instituto de Aeronáutica e Espaço, São José dos Campos, Brazil  
joaoluiz.azevedo@gmail.com, humbertoham@iae.cta.br, edsonbss@gmail.com, damilano@iae.cta.br

**Abstract.** *The present work deals with the calculation of wall heat fluxes over the small ballistic reentry Brazilian vehicle SARA (acronym for Satélite de Reentrada Atmosférica). The results of the present investigation will be used in the future to size the thermal protection material that will have to be added to the SARA configuration in order to guarantee the integrity of the vehicle during its flight. Experimental data such as altitude and velocity of the vehicle were calculated at different positions of the launch trajectory at Instituto de Aeronáutica e Espaço (IAE). Numerical simulations of the compressible flow over the ballistic vehicle are performed in order to correctly compute the heat transfer at the wall. The flight trajectory data are used as boundary conditions for the numerical simulations. During the portion of the trajectory of interest here, the Mach number ranges from 0.5 to 7.8, and the altitude from 0.5 km to 56 km. For all simulations performed in the present work, the dimensionless distance of the wall of the first mesh cell is less than one. Therefore, one mesh was created for each position along the launch trajectory, because the mesh is dependent on the Reynolds number. The numerical results are used as a reference to validate engineering calculations of the SARA heat transfer rates. At this point, the plans for the sub-orbital SARA capsule flight are such that it will fly without any wind tunnel validation of the heat fluxes here determined.*

**Keywords:** *CFD, Sounding rockets, Heat transfer, High speed flows, SARA.*

### 1. INTRODUCTION

Space and sub-orbital vehicles reach high velocities within atmosphere, about 100 km over the surface of Earth. Such high velocities result in aerodynamic heating and air temperature surpasses 2000° C at the stagnation point. Besides the effects of high temperatures on the mechanical behavior of the structure and on-board devices, it is mandatory to preserve the payload, by using an efficient TPS (Thermal Protection System). As a consequence, TPS design is a critical aspect of a rocket design, since his under dimensioning may result in the loss of the payload and the over dimensioning implies in increasing weight and cost.

This work focusses on the validation of an engineering method (Zoby *et al.*, 1981) to predict the wall heat fluxes over the small ballistic reentry Brazilian vehicle SARA (acronym for Satélite de Reentrada Atmosférica) for laminar flow configurations. The normal heat flux of ten different positions of the SARA trajectory are calculated using the method of Zoby and the LeMans code, which is an already validated CFD solver (Scalabrin, 2007). The results obtained by both methods are compared and discussed in the present paper.

### 2. ENGINEERING CALCULATION METHOD

To predict the heat transfer on SARA, it is necessary to know pressure, temperature and velocity fields around the vehicle. That can be accomplished by numerically solving the Navier-Stokes equations. However, such a procedure is expensive and time consuming. In the present work a simpler, but reliable, engineering approach is also used. The following simplifying assumptions are made:

- Zero angle of attack;
- SARA rotation around its longitudinal axis is neglected;

- Atmospheric air is considered to behave as a calorically and thermally perfect gas (no chemical reactions); and the free stream conditions ahead of the nose cap are those given by  $v_\infty$ ,  $T_\infty$ ,  $p_\infty$ , corresponding, respectively, to velocity, temperature and pressure. By knowing  $v_\infty$  and altitude, as function of time, together with atmospheric model (NOAA - National Oceanic and Atmospheric Administration, 1976), it is possible to evaluate the free stream properties, such as  $p_\infty$ ,  $T_\infty$  and  $c_\infty$ , which represent free stream pressure, temperature and speed of sound, respectively. For supersonic flow ( $M_\infty > 1$ ), a detached shock wave appears ahead of the nose. By using the normal shock relationships, it is possible to calculate  $v_1$ ,  $T_1$ ,  $p_1$  after the shock.

The heat flux over the external surface was calculated through the Zoby's method (Zoby *et al.*, 1981; Miranda and Mayall, 2001), namely:

$$q = H (T_{aw} - T_w) \quad (1)$$

where  $q$  is heat flux,  $T_w$  is the wall temperature and  $T_{aw}$  is the adiabatic wall temperature, also called recovery temperature,  $T_w$ , given by:

$$T_{aw} = T_e + F_R \frac{v_e^2}{2c_p} \quad (2)$$

where  $c_p$  is the specific heat,  $T_e$  the temperature and  $v_e$  the velocity. The subscript  $e$  refers to conditions at the boundary layer edge.  $F_R$  is the recovery factor, equal to  $\sqrt{Pr_w}$ , for laminar flow and  $\sqrt[3]{Pr_w}$  for turbulent flow.  $Pr_w$  is the Prandtl number evaluated at wall temperature,  $Pr_w = 0.71$ . The convective heat transfer coefficient comes from the Reynolds analogy, namely:

$$H = 0.5 \rho_e c_p v_e Pr_w^{-a} C_f \quad (3)$$

where  $a$  is equal to 0.6 for laminar flows and 0.4 for turbulent flows. To take into account compressibility effects, a modified friction factor is obtained (Anderson, 1989).

$$C_F = K_1 (Re_\theta)^{K_2} \left( \frac{\rho_e^*}{\rho_e} \right)^{K_3} \left( \frac{\mu_e^*}{\mu_e} \right)^{K_3} \quad (4)$$

In the equation (4),  $Re_\theta$  is the Reynolds number, based on the boundary layer thickness,  $\theta$ .

$$Re_\theta = \frac{\rho_e v_e \theta}{\mu_e} \quad (5)$$

The superscript  $*$  refers to properties evaluated at Eckert's reference temperature ( $T_e^*$ ). Viscosity,  $\mu$ , is evaluated according to Sutherland's equation, as function of temperature (Anderson, 1989) and  $\rho$  is the specific mass. In Eq. (4)  $K_1 = 0.44$ ,  $K_2 = -1$  and  $K_3 = 1$ , for laminar flow. For turbulent flow,  $K_2 = K_3 = -m$ , and

$$K_1 = 2 \left( \frac{1}{C_5} \right)^{\frac{2N}{N+1}} \left[ \frac{N}{(N+1)(N+2)} \right]^m \quad (6a)$$

$$m = \frac{2}{N+1} \quad (6b)$$

$$C_5 = 2.2433 + 0.93N \quad (6c)$$

$$N = 12.76 - 6.5 \log_{10}(Re_\theta) + 1.21 [\log_{10}(Re_\theta)]^2 \quad (6d)$$

For laminar flow, the boundary layer thickness is given by (Anderson, 1989):

$$\theta_l = \frac{0.664 \left( \int_0^y \rho_e^* \mu_e^* v_e^* R^2 dy' \right)^{\frac{1}{2}}}{\rho_e v_e R} \quad (7)$$

where  $y$  is measured along the surface of the body and  $y = 0$  corresponds to the stagnation point, and  $R$  is a geometric parameter schematically shown in Fig. 1, where the curved red line represents the nose cap surface. In this work the numer-

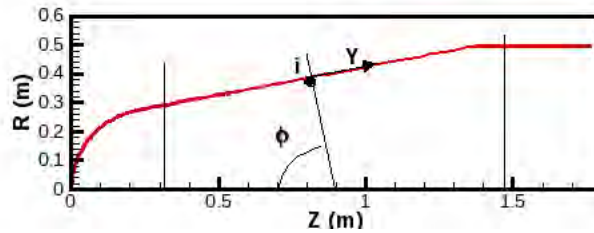


Figure 1. Coordinate system

ical integration of Eq. (7) was obtained according to the trapezoidal method. As  $R \rightarrow 0$ , Eq. (7) becomes undetermined. By taking the limit of Eq. (7) as  $R \rightarrow 0$ , the following expression is obtained (Miranda and Mayall, 2001):

$$\theta_l = \frac{0.332 (\rho_e^* \mu_e^*)^{\frac{1}{2}}}{\rho_e \sqrt{\frac{1}{R_N} \left[ \frac{2(p_s - p_\infty)}{p_s} \right]^{\frac{1}{2}}}} \quad (8)$$

In this work Eq. (8) is applied for  $y < 0.1R_N$ , where  $R_N$  is the radius of curvature at the stagnation point.

The boundary layer thickness for turbulent flow is obtained by solving the following first order differential equation:

$$\frac{D(\rho_e v_e R \theta_T)}{Dy} = 0.5 C_F \rho_e v_e R \quad (9)$$

After obtaining the boundary layer momentum thickness,  $\theta$ ,  $Re_\theta$ ,  $C_F$  and  $H$  can be evaluated by using Eqs. (5), (4) and (3), respectively. Along the transition region between laminar and turbulent flow, the following relationship is used:

$$q_{Tr} = q_L + F(y) (q_T - q_L) \quad (10)$$

where the subscripts  $Tr$ ,  $L$  and  $T$  represent, respectively, transitional, laminar and turbulent flow. The transitional factor,  $F(y)$ , is given by (Dhawan and Narasimha, 1958):

$$F(y) = 1 - \exp \left\{ -0.412 \left[ \frac{4.74(y - y_L)}{(y_T - y_L)} \right] \right\} \quad (11)$$

Transition is supposed to occur for  $163 < Re_\theta < 275$ .

Properties evaluation at the boundary layer edge is performed assuming isentropic flow between the stagnation region and the location 'i' where properties are needed, namely

$$\rho_{e,i} = \rho_s \left( \frac{p_{e,i}}{p_s} \right)^{\frac{1}{\gamma}} ; \quad h_{e,i} = h_s \left( \frac{p_{e,i}}{p_s} \right)^{\frac{\gamma-1}{\gamma}} ; \quad v_{e,i} = \sqrt{2(h_s - h_{e,i})} ; \quad T_{e,i} = \frac{h_{e,i}}{c_p} \quad (12)$$

The local pressure,  $p_{e,i}$ , is obtained from the modified Newton's method (Anderson, 1989; Machado and Villas-Boas, 2006) and  $\gamma = 1.4$ . The results of both methods are then compared. The subscript 's' appearing in Eq. (12) refers to the stagnation condition. Eckert's reference temperature is obtained from (Anderson, 1989):

$$\frac{T_{e,i}^*}{T_{e,i}} = 1 + 0.032 M_{e,i}^2 + 0.58 \left( \frac{T_W}{T_{e,i}} - 1 \right) \quad (13)$$

The solution procedure can be summarized as follows:

1. From a given trajectory the US Standard Atmosphere (1976) is used to obtain the free stream properties, including the stagnation ones;
2. Normal shock relationships are used to obtain the fluid flow properties behind the shock;
3. By using the modified Newton method, pressure distribution is obtained along the payload;
4. Equation (12) provide the local properties at the boundary layer edge;
5. If  $y < 0.1 R_N$ , Eq. (9) provides the laminar boundary layer thickness, leading to the estimation of  $Re_\theta$ ,  $C_F$  and  $H$ , provided by Eqs. (5), (4) and (3), respectively;

6. If  $y > 0.1 R_N$  and  $Re_\theta < 163$ , Eq. (7) is numerically integrated up to the location where the momentum thickness is to be estimated. Such an integration is performed by using the trapezoidal method;
7. If  $y > 0.1 R_N$  and  $Re_\theta > 275$ , Eq. (9) is numerically integrated by the trapezoidal rule leading to the turbulent boundary layer thickness;
8. If  $y > 0.1 R_N$  and  $163 < Re_\theta < 275$ , Eqs. (10) and (11) are used to estimate H;

It should be pointed out that such a procedure is performed along the payload surface (following the y-coordinate), for different trajectory times. Therefore,  $H = H(y, t)$ .

### 3. NUMERICAL FORMULATION

The numerical formulation applied in this work is briefly presented in this section. All the study is performed using the Reynolds-averaged Navier-Stokes equations. The set of equations is written here in the context of a cell-centered finite-volume formulation as

$$\frac{\partial Q_i}{\partial t} = -\frac{1}{V_i} \sum_{k=1}^{nf} \vec{F}_k \cdot \vec{n}_k S_k. \quad (14)$$

in which,  $Q$ , is the vector of conservative properties,  $V$ , is the volume of the cell,  $F$ , is the numerical flux through the faces of the cell,  $\vec{n}$ , is the outward normal face vector, and  $S$ , is the surface of the face. The subscripts,  $k$  and  $i$ , indicate the face index and cells index, respectively and the superscript  $nf$  indicates the number of faces of the  $i$ -th cell.

#### 3.1 Inviscid flux calculation

The inviscid fluxes are calculated using a method based on a classical flux vector splitting formulation, the Steger-Warming scheme (Steger and Warming, 1981). This method is an upwind scheme that uses the homogeneous property of the inviscid flux vectors. The flux vector splitting separates the flux into two parts, the downstream and the upstream flux, in relation to the face orientation as

$$\vec{F} \cdot \vec{n} = F_n^+ + F_n^- = (A_{cl}^+ Q_{cl} + A_{cr}^- Q_{cr}), \quad (15)$$

where  $F_n$  is the normal flux at the  $k$ -th face, and  $A$  is the Jacobian matrix of the inviscid flux that. The  $cl$  and  $cr$  subscripts are the cells on the left and right sides of the face. Numerical studies indicate that this flux vector splitting is too dissipative and it can deteriorate the boundary layer profiles (MacCormack and Candler, 1989; Junqueira-Junior *et al.*, 2011; Junqueira-Junior, 2012; Scalabrin, 2007). Therefore, a pressure switch is used to smoothly shift the Steger-Warming scheme into a centered one. Hence, the artificial dissipation is controlled and the numerical stability is maintained. The modified formulation can be written as

$$\vec{F}_k \cdot \vec{n}_k = F_k^+ + F_k^- = (A_{k+}^+ Q_{k+} + A_{k-}^- Q_{k-}) \quad (16)$$

in which

$$Q_{k+} = (1 - w) Q_{cl} + w Q_{cr} \quad \text{and} \quad Q_{k-} = (1 - w) Q_{cr} + w Q_{cl}. \quad (17)$$

The switch,  $w$ , is given by

$$w = \frac{1}{2} \frac{1}{(\alpha \nabla p)^2 + 1} \quad \text{and} \quad \nabla p = \frac{|p_{cl} - p_{cr}|}{\min(p_{cl}, p_{cr})}. \quad (18)$$

Therefore, for small  $\nabla p$ ,  $w = (1 - w) = 0.5$ , and the code runs with a centered scheme. For large values of  $\nabla p$ ,  $w = 0$  and  $(1 - w) = 1$ , and the code runs with the standard Steger-Warming scheme. For Eq. (18), the literature suggests using  $\alpha = 6$ , but some problems may require larger values (Scalabrin, 2007).

#### 3.2 Viscous flux calculation

The viscous terms are based on derivative of properties on the faces. To build the derivative terms, two volumes are created over the face where the derivative is being calculated. At the center of each new volume, the derivative is calculated using the Green-Gauss theorem. This computation is used to find the derivative at the desired face. The work of Scalabrin (2007) and of Junqueira-Junior (2012) provide further details on the viscous flux computations.

### 3.3 Point implicit integration

The implicit integration method applied in this work is based on the backward Euler method (Lomax *et al.*, 2001). One can apply the spatial discretization and the face-based notation in order to write the set of equations as

$$\left[ \frac{V_{cl}}{\Delta t} + \sum_{k=1}^{nf} A_{k+}^+ S_k \right] \Delta Q_{cl}^n + \sum_{k=1}^{nf} A_{k-}^- S_k \Delta Q_{cr,k}^n = R_{cl}^n. \quad (19)$$

In a simpler form, one can write

$$[M] \Delta Q_{cl}^n + \frac{V_{cl}}{\Delta t} [I] \Delta Q_{cl}^n = R_{cl}^n. \quad (20)$$

The implicit integration of unstructured meshes is very expensive and, in most cases, impractical, because it generates very large sparse linear systems. An approximate method, the point-implicit integration, is applied in the present work (Scalabrin, 2007; Junqueira-Junior, 2012). For this time-marching method, the  $[M]$  matrix, presented in Eq. (20), is split into a diagonal matrix,  $[M]_d$ , and an off-diagonal matrix,  $[M]_{od}$ , as

$$[M] = [M]_d + [M]_{od}. \quad (21)$$

Then, the linear system is written as

$$[M]_d \Delta Q_{cl}^p + \frac{V_{cl}}{\Delta t} [I] \Delta Q_{cl}^p = R_{cl}^n - [M]_{od} \Delta Q_{cl}^{p-1}. \quad (22)$$

The point-implicit method performs sub-iterations, in  $p$ , until a predefined number of sub-iterations or until the convergence of  $\Delta Q_{cl}$ . The sub-iterations are started assuming that  $\Delta Q_{cl}^0 = 0$ .

### 3.4 Second Order Extension of Inviscid Fluxes

The monotone upstream-centered scheme for conservation laws, known as MUSCL approach (van Leer, 1979), is used in the present work in order to obtain second order extension for the inviscid fluxes calculation. The MUSCL variable extrapolation for 2D, or 3D, is straightforward for structured meshes. However it is not very simple for unstructured solvers. In the present work, the stencils were created using only cell centered values for second order reconstruction. The work of Scalabrin (2007) and Junqueira-Junior (2012) present further informations about the stencil search on unstructured grids and the numerical formulation of the second order reconstruction.

## 4. RESULTS

Numerical simulations are performed to evaluate the heat flux normal to the wall for different positions of the SARA trajectory. The flight conditions and the Reynolds number for different positions of the trajectory are presented in Tab. 1. The freestream properties are calculated using the (NOAA - National Oceanic and Atmospheric Administration, 1976). Figure 2 presents the geometry and the boundary conditions used for the flow simulations. Wall boundary condition, with fixed temperature at  $300\text{ K}$  and no slip condition is defined over the SARA surface. The temperature of  $300\text{ K}$  is specified by designers of the reentry Brazilian vehicle. Far-field boundary condition is set at the entry and the exit of the computational domain. Riemann invariants are implemented in order to calculate the sign of the eigen value at the far-field boundaries and correctly predict the direction of the propagation of data. Axi-symmetric boundary condition is applied at the bottom of the computational domain. This boundary condition enables the correct study of a three dimensional flow using a two dimensional domain. One different mesh is created of each simulation performed in the present work. Figure 3 presents the mesh designed for last six points of the SARA trajectory. The dimensionless normal distance of the first cell to the wall,  $y^+$ , is approximately one for all simulation configurations and the size of the meshes used here are the order of 25.000 cells. In this work the turbulence modeling of the CFD solver is switched off to validate the laminar formulation of the engineering method of Zoby *et al.* (1981).

C. A. Junqueira-Junior, F. R. C. Barreto, J. L. F. Azevedo, H. A. Machado, E. Basso and G. Damilano  
Calculation of Wall Heat Fluxes for the Sub-Orbital SARA Capsule Atmospheric Flight

Table 1. Freestream flow conditions at different positions along the trajectory

| Time [s] | Altitude [Km] | Velocity [m/s] | Mach Number | Reynolds Number |
|----------|---------------|----------------|-------------|-----------------|
| 15       | 1.919         | 379.005        | 1.139       | 3.78E+07        |
| 18       | 6.043         | 668.211        | 2.113       | 3.85E+07        |
| 20       | 7.431         | 743.835        | 2.396       | 3.78E+07        |
| 23       | 9.799         | 864.573        | 2.878       | 3.50E+07        |
| 25       | 11.580        | 952.139        | 3.227       | 2.25E+07        |
| 30       | 16.876        | 1223.357       | 4.146       | 1.74E+07        |
| 35       | 23.732        | 1600.470       | 5.379       | 7.85E+06        |
| 40       | 32.783        | 2130.363       | 7.002       | 2.38E+06        |
| 45       | 44.159        | 2463.111       | 7.593       | 4.76E+05        |
| 50       | 56.442        | 2543.016       | 7.826       | 1.00E+05        |

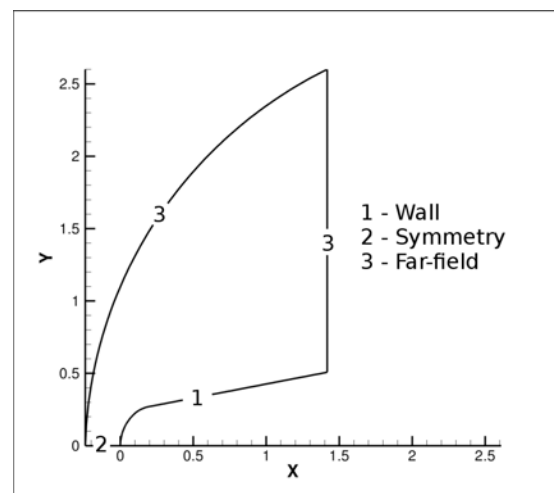


Figure 2. Geometry and boundary conditions of the sub-orbital platform

Figures 4 and 5 present the distributions of Mach number and temperature of different points of the trajectory, from 25 to 50 seconds. Figures 6 and 7 present the normal heat flux along the SARA wall surface at different positions of the trajectory calculated using the engineering method and the CFD solver. One can state that for higher Reynolds number the difference between the CFD solution and the method of Zoby is more significative. For the flight conditions at 45 seconds and 50 seconds, in which the flow cannot be considered as a turbulent flow, there is a great accordance between the two methods compared in the present article. These two configurations are very important to initiate the validation process of the method of Zoby. However, one can point here that, it is of most importance to validate the formulation of Zoby for other flow conditions. Until 40 seconds of the trajectory, the flow conditions can be considered as turbulent. Moreover, the dissociation of oxygen cannot be neglected for altitudes higher than 40 kilometers and temperatures higher than 2500 Kelvin. Such conditions are present at two points of the flight, 45 and 50 seconds of the trajectory. Therefore, turbulent and chemical reaction effects have to be considered for the full validation of the fomulation of Zoby. It is also very important to point here that, for all studies performed in the present work, the engineering method underpredicted the normal heat flux along the SARA surface. More studies should be performed in order to evaluate the effects of such behavior.

22nd International Congress of Mechanical Engineering (COBEM 2013)  
November 3-7, 2013, Ribeirão Preto, SP, Brazil

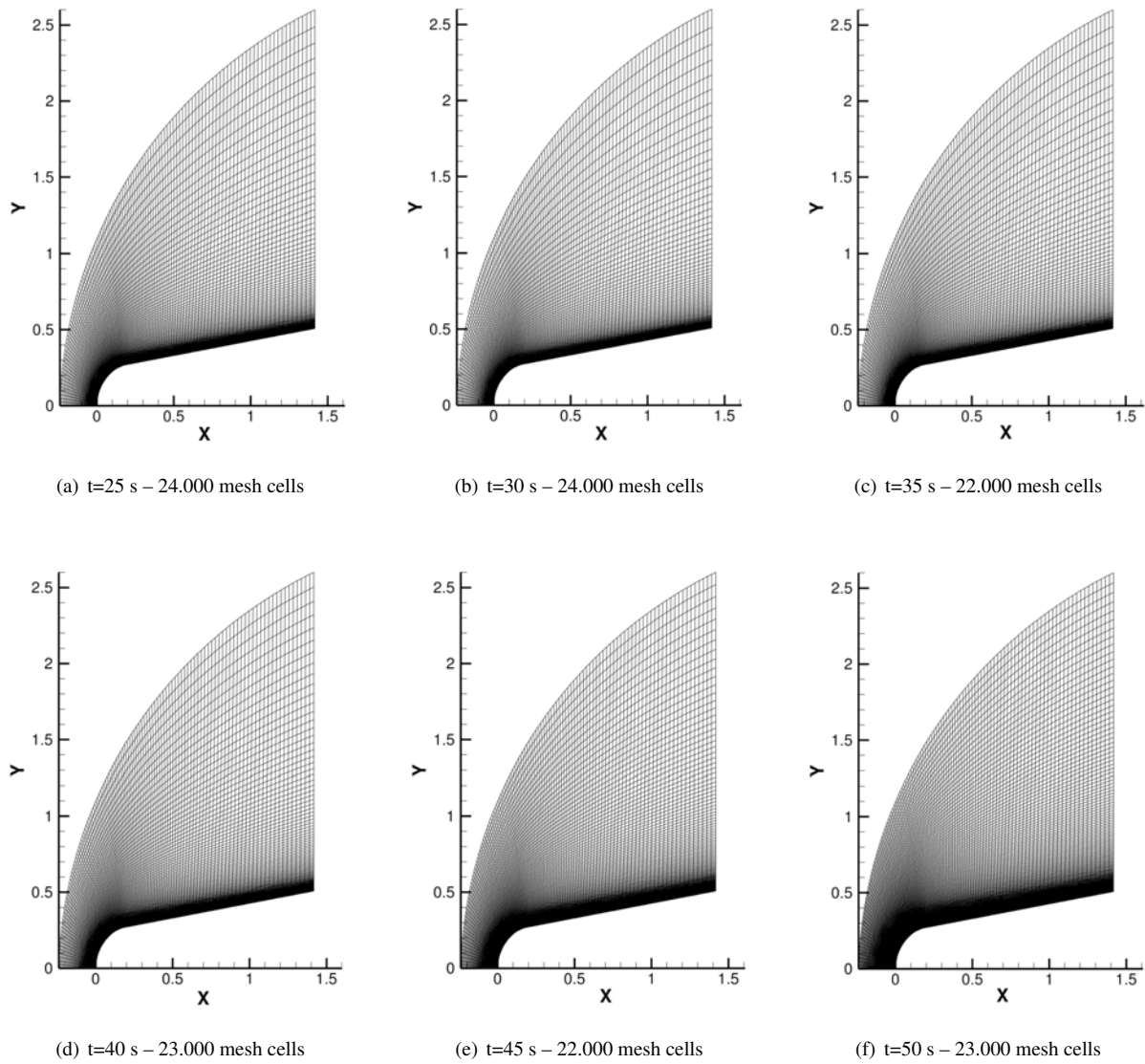
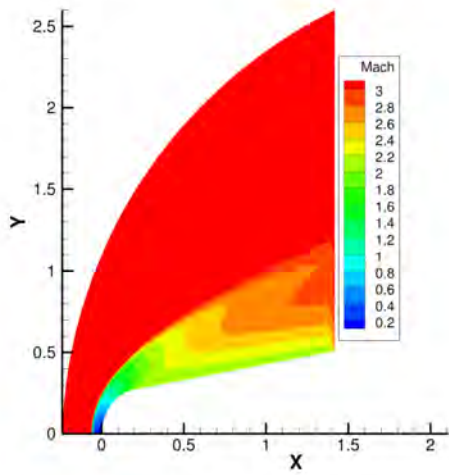
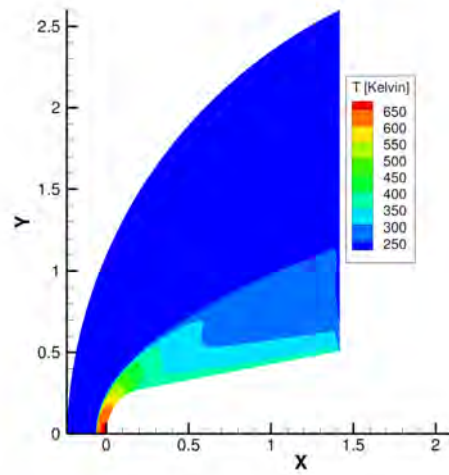


Figure 3. Meshes used for the simulations of the four last points of the trajectory

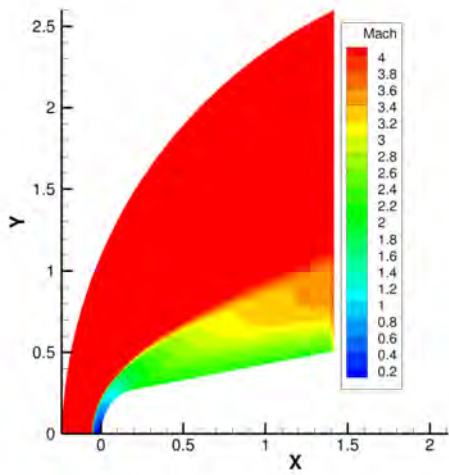
C. A. Junqueira-Junior, F. R. C. Barreto, J. L. F. Azevedo, H. A. Machado, E. Basso and G. Damilano  
 Calculation of Wall Heat Fluxes for the Sub-Orbital SARA Capsule Atmospheric Flight



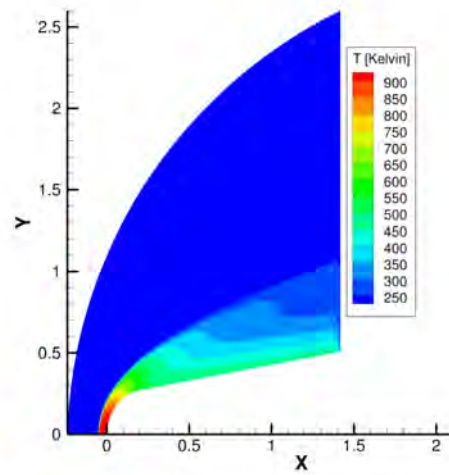
(a) t=25 s – Mach number



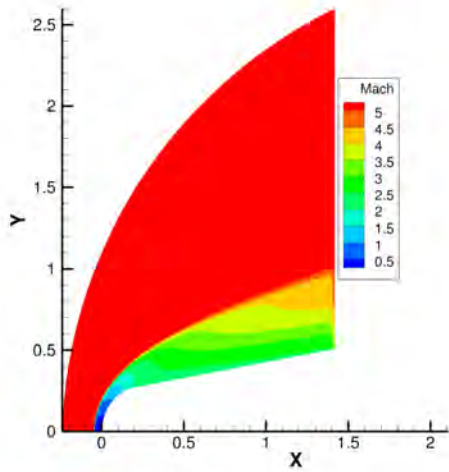
(b) t=25 s – Temperature



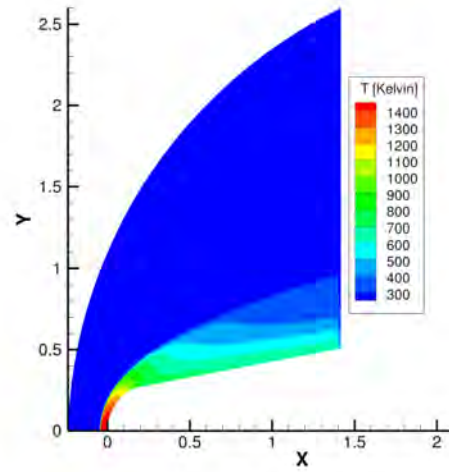
(c) t=30 s – Mach number



(d) t=30 s – Temperature



(e) t=35 s – Mach number



(f) t=35 s – Temperature

Figure 4. Mach number and temperature distributions 25, 30 and 35 seconds of trajectory

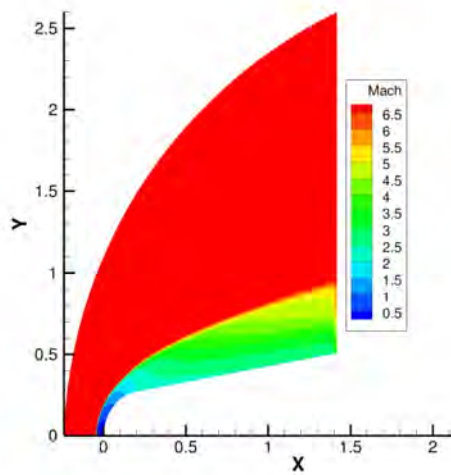
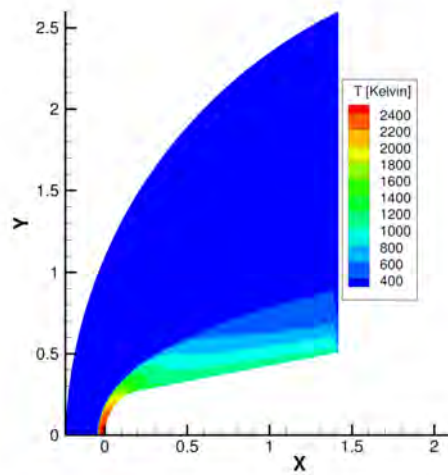
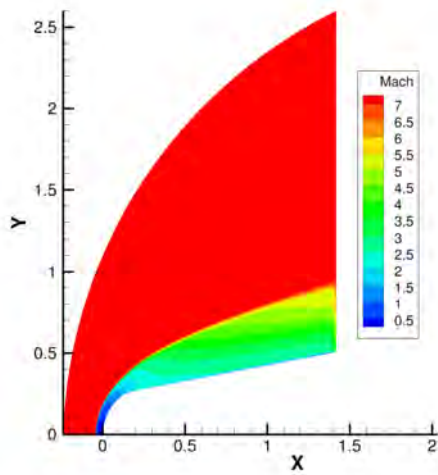
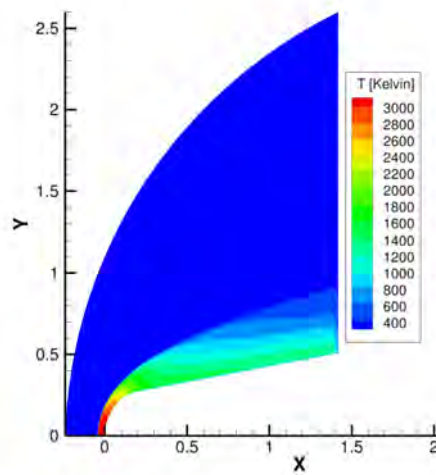
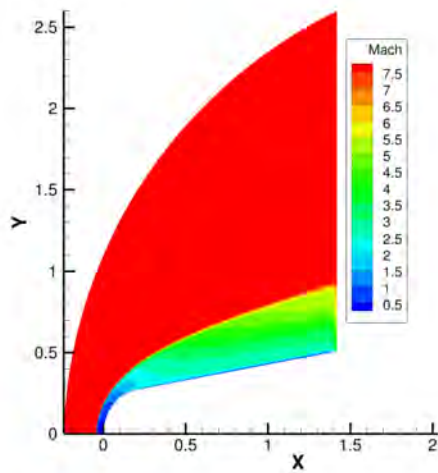
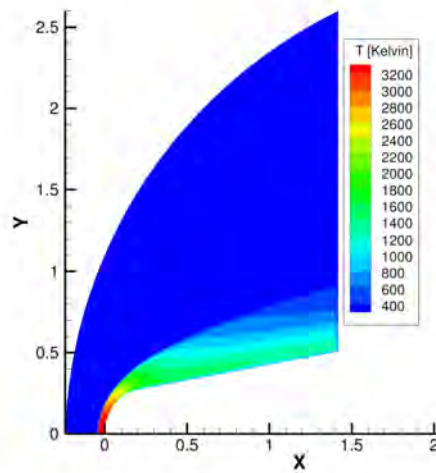
(a)  $t=40$  s – Mach number(b)  $t=40$  s – Temperature(c)  $t=45$  s – Mach number(d)  $t=45$  s – Temperature(e)  $t=50$  s – Mach number(f)  $t=50$  s – Temperature

Figure 5. Mach number and temperature distributions 40, 45 and 50 seconds of trajectory

C. A. Junqueira-Junior, F. R. C. Barreto, J. L. F. Azevedo, H. A. Machado, E. Basso and G. Damilano  
Calculation of Wall Heat Fluxes for the Sub-Orbital SARA Capsule Atmospheric Flight

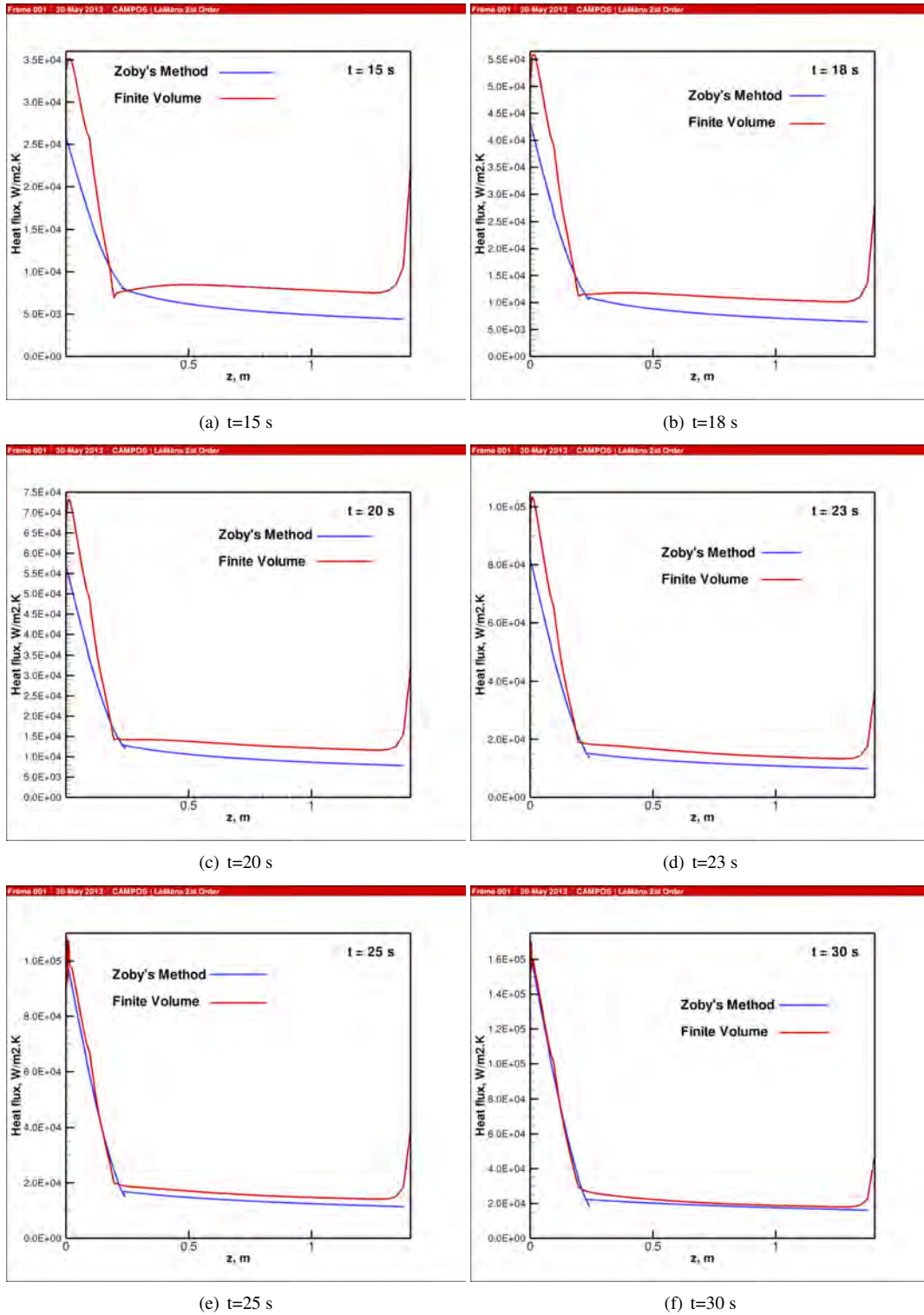


Figure 6. Comparison of the normal heat flux along the SARA wall surface for the first six points of the trajectory

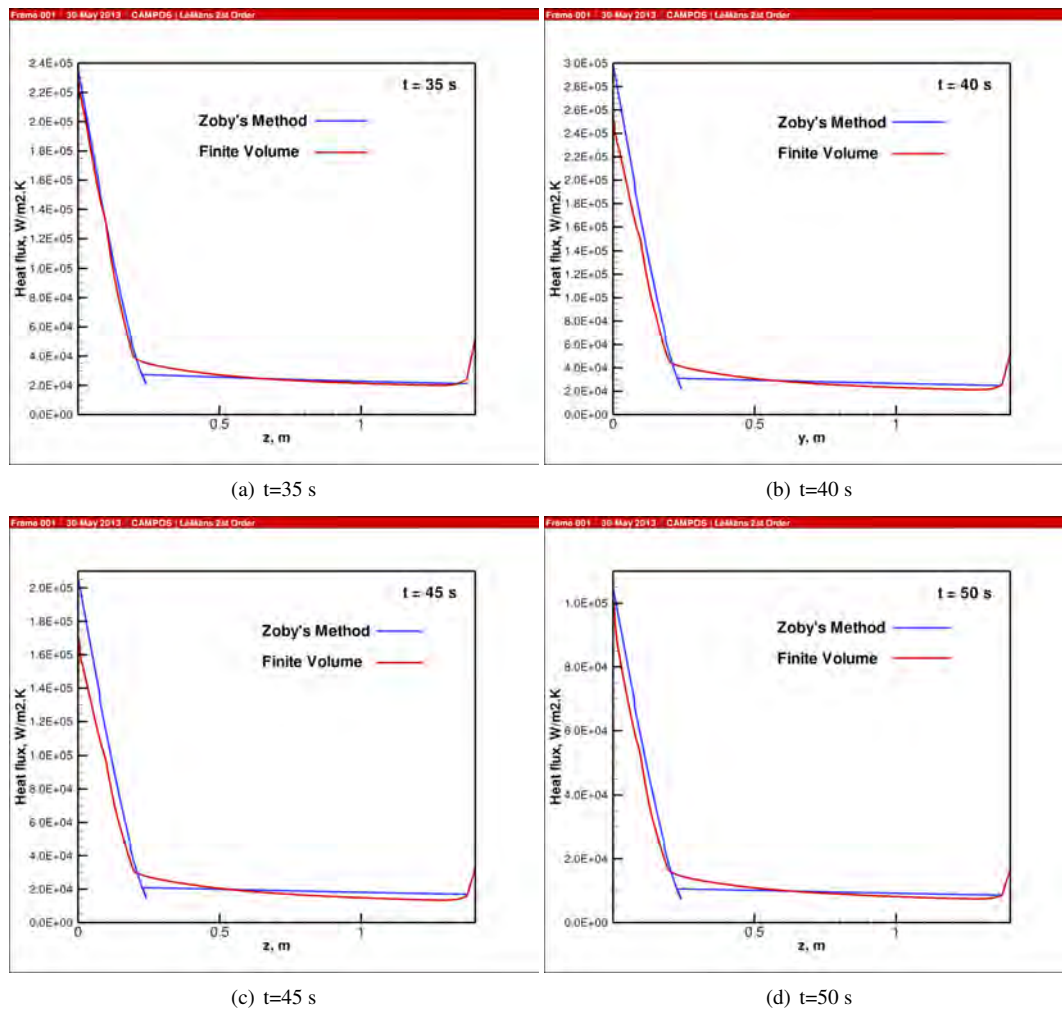


Figure 7. Comparison of the normal heat flux along the SARA wall surface for the last four points of the trajectory

## 5. CONCLUSION

The present work presents the comparison of the normal heat flux at different positions of the trajectory of the small ballistic reentry Brazilian vehicle using two different approaches, CFD simulations and the method of Zoby. The numerical simulations are used as references to validate the laminar formulation of the engineering method.

Results indicate that for low altitude conditions, in which the Reynolds number is higher, and the flow is considered turbulent, the difference between the heat flux computed by the two methods is significant. However, for higher altitude and lower density configurations, in which the flow cannot be considered as a turbulent flow, the results of the two methods are in great accordance. This agreement is very important since only the laminar formulation of the method of Zoby is compared in this work. Nevertheless, more studies of laminar flows configurations are necessary in order to evaluate the method of Zoby. It is also very important to calculate the heat flux over the SARA surface using numerical simulations with turbulence closures and chemical reaction formulations. Then, the numerical results should be compared with the results of the method of Zoby with a turbulent and chemical reaction approach. Only after the proposed studies one can validate the engineering method for wall heat flux calculations.

## 6. ACKNOWLEDGEMENTS

The authors would like to acknowledge Conselho Nacional de Desenvolvimento Científico e Tecnológico, CNPq, which partially supported the project under the Research Grants No. 312064/2006-3, No. 471592/2011-0 and No. 479140/2011-1. Further partial support was provided by Fundação Coordenação de Aperfeiçoamento de Pessoal de Nível Superior, CAPES, through a Ph.D. scholarship to the first author, and it is also gratefully acknowledged.

C. A. Junqueira-Junior, F. R. C. Barreto, J. L. F. Azevedo, H. A. Machado, E. Basso and G. Damilano  
Calculation of Wall Heat Fluxes for the Sub-Orbital SARA Capsule Atmospheric Flight

## 7. REFERENCES

- Anderson, J.D.J., 1989. *Hypersonic and High Temperature Gas Dynamics*. AIAA Education Series. AIAA, New York, NY, USA.
- Dhawan, S. and Narasimha, R., 1958. “Some properties of boundary layer flow during the transition from laminar to turbulent motion”. *Journal of Fluid Mechanics*, Vol. 3, No. 04, pp. 418–436.
- Junqueira-Junior, C.A., 2012. *A study on the extension of an upwind parallel solver for turbulent flow applications*. M.S. thesis, Instituto Tecnológico de Aeronáutica, São José dos Campos, Brazil.
- Junqueira-Junior, C.A., Azevedo, J.L.F., Basso, E. and Scalabrin, L.C., 2011. “Study of robust and efficient turbulence closures for aerospace applications”. In *Proceedings of the Iberian Latin American Congress on Computational Methods in Engineering - CILAMCE XXXII*. Ouro Preto, Brazil.
- Lomax, H., Pulliam, T.H. and Zingg, D.W., 2001. *Fundamentals of Computation Fluid Dynamics*. Springer, New York, USA, 1st edition.
- MacCormack, R.W. and Candler, G.V., 1989. “The solution of the Navier-Stokes equations using Gauss-Seidel line relaxation”. *Computer and Fluids*, Vol. 17, No. 1, pp. 135–150.
- Machado, H.A. and Villas-Boas, D.J.F., 2006. “Comparative study of models for aerodynamic heating of space vehicles”. In *Proceedings of the 11th Brazilian Congress of Thermal Sciences and Engineering*. Curitiba, Brazil (in Portuguese, original title is “Estudo comparativo de modelos para aquecimento aerodinâmico de veículos espaciais”).
- Miranda, I.F. and Mayall, M., 2001. *Convective Heat Flux in Micro-Satellites during the Atmospheric Reentry*. Graduation project, Instituto Tecnológico de Aeronáutica – ITA, São José dos Campos, Brazil.
- NOAA - National Oceanic and Atmospheric Administration, 1976. *U.S. Standard Atmosphere, 1976*. U.S. Government Printing Office, Washington, D.C., USA.
- Scalabrin, L.C., 2007. *Numerical simulation of weakly ionized hypersonic flow over reentry capsules*. Ph.D. thesis, University of Michigan, Michigan, USA.
- Steger, J.L. and Warming, R.F., 1981. “Flux vector splitting of the inviscid gasdynamic equations with application to the finite-difference method”. *Journal of Computational Physics*, Vol. 40, pp. 263–293.
- Zoby, E.V., Moss, J.N. and Sutton, K., 1981. “Approximate convective heat equations hypersonic flows”. *Journal of Spacecraft and Rockets*, Vol. 18, No. 1, pp. 64–70.

## 8. RESPONSIBILITY NOTICE

The authors are the only responsible for the printed material included in this paper.